Int. J. Electrochem. Sci., 16 **(2021)** Article ID: 210712, doi: 10.20964/2021.07.17

International Journal of
ELECTROCHEMICAL
SCIENCE
www.electrochemsci.org

Impedimetric multifunctional Sensor Based on Rubber-CNTs-orange Dye Nanocomposite Fabricated by Rubbing-in Technology

Muhammad Tariq Saeed Chani[1,2,], Khasan S. Karimov[3,4], Hadi M. Marwani[1,2], Hafiz Muhammad Zeeshan[3], Mohammed M. Rahman[1,2], Abdullah M. Asiri[1,2]*

[1] Center of Excellence for Advanced Materials Research, King Abdulaziz University, Jeddah 21589, P.O. Box 80203, Saudi Arabia
[2] Chemistry Department, Faculty of Science, King Abdulaziz University, Jeddah 21589, P.O. Box 80203, Saudi Arabia
[3] Ghulam Ishaq Khan Institute of Engineering Sciences and Technology, Topi-23640, KPK, Pakistan
[4] Center for Innovative Development of Science and Technologies of Academy of Sciences, Rudaki Ave., 33, Dushanbe, 734025, Tajikistan
[*]E-mail: tariqchani1@gmail.com, tariq_chani@yahoo.com

Received: 3 March 2021 / *Accepted:* 15 April 2021 / *Published:* 31 May 2021

This study presents the fabrication and investigation of rubber-carbon nanotubes-orange dye (rubber-CNTs-OD) nanocomposite based resistive and impedimetric sensors. These shockproof multifunctional sensors may be used for displacement, pressure, force, humidity and temperature sensing. Rubbing-in technology was used to fabricate the coplanar sensors on rubber substrates of dimensions 12x5x5 mm^3. In the middle of the substrates, the OD-CNTs mixture (1:1 wt.%) was rubbed-in to make 3 mm wide and 12-18 µm deep active layer. On both sides of the active layer the rubber-CNTs layers were formed, that act as conductive electrodes. The length, width and the thickness of the electrodes were 4-5 mm, 5 mm and 12-18 µm, respectively. The resistance and the impedance of the sensors decreased under the effect of compressive displacement, pressure, humidity and temperature. These reductions were -43 Ω/µm to -73 Ω/µm, -3950 Ω-cm^2/kgf to -6008 Ω-cm^2/kgf, -187 Ω/%RH to -981 Ω/%RH and -216 Ω/°C to -270 Ω/°C, respectively. The force (in perpendicular direction to the length) causes to increase the resistance and impedance (60 Ω/gf to 300 Ω/gf). The probable reasons of the observed changes in the resistance and impedance of the sensor have been described.

Keywords: Semiconductor; Shockproof; Displacement sensor; Force sensor; Pressure sensor; Humidity sensor; Temperature sensor.

1. INTRODUCTION

At present different kinds of sensor are used in practice which measure the force, displacement, pressure, etc., Force, displacement and acceleration sensors were described in Ref. [1]. The structure and the properties of the capacitive pressure sensor with a mechanical force-displacement transducer based on CMOS-MEMS were described in Ref. [2]. These sensors are based on deformable diaphragm with embedded fixed and moveable electrodes. The diaphragm deforms under the effect of pressure and electrode moves, which causes to change the capacitance. They also proposed various designs to improve the sensitivity up to 126% in the pressure range of 20kPa to 300 kPa. The Ref [3] described the design and the characterization of a tactile sensors (magnetic Hall effect sensor) for application in splints. This 3mm thick and 4mm radius sensor has normal and shear pressure sensing range up to 44.0 kPa and 6.0 kPa, respectively. Reference [4] presented a tactile sensor (based on flexible polymer) containing embedded capacitors (multiple) for the measurement of shear and normal force. The single sensor's full-scale detectable range is 10 mN in x-, y- and z-directions and the maximum sensitivity is up to 3.0%/mN. The ref. [5] described the force-sensing resistor array using method of resolution enhancement. A flexible piezoelectric (lead-free) transducer was developed for health monitoring in the space [6].

For the measurement and detection of environmental parameters the methods and apparatus were described in Ref. [7] where it was provided a device for the recording and in-situ measurements of different parameters (environmental) in the manufacturing processes like semiconductors devices fabrication. For the remote measurement of environmental parameters and power system (beyond line-of-site) a line-mounted apparatus was described [8]. The modules of the sensors in this apparatus have the capability to measure environmental or mechanical and electrical parameters near the high voltage conductor. Ref. [9] presented a smart sensing (Zigbee based) platform to monitor various environmental parameters. To measure and monitor the environmental parameters the electromagnetic (planar) sensors were developed and described in ref. [10].

The structure-property relationship in silicon rubber nanocomposites reinforced with carbon nanomaterials for sensor and actuators was investigated [11]. Particularly, preparation of rubber-nanocomposites with carbon black (0-dimensional (0-D)), CNTs (1-D), graphitic nanofiller (3-D) and silicone rubber (room temperature vulcanized (RTV)). The application of carbon nanofillers in sensors and actuators were discussed in ref. [12]: the RTV rubber and various nanofillers were mixed to prepare nanocomposites for various industrial applications. The RTV rubber and HTV (high-temperature vulcanized) rubber composites with CNTs were prepared also for sensors and actuators [13].

The graphene and CNTs powers-based multifunctional sensors were fabricated and investigated for the measurement of displacement, pressure and gradient temperature [14]. Number of papers was published by us during last years on the investigation of sensors properties. Particularly, investigation flexible multifunctional sensors based on graphene-rubber nanocomposite [15], and humidity sensing properties of the OD-graphene solid-electrolyte-based cells [16].

In continuation of our efforts for the fabrication and investigation of sensors [14, 17-32], here we are presenting the data about the displacement, pressure, force, humidity and temperature sensing

characteristics of the rubber-CNTs-OD nanocomposite-based multifunctional sensors. These sensors were fabricated by rubbing-in technology and their sensing mechanism is based on change in resistance and impedance.

2. EXPERIMENTAL

For the fabrication of sensors, the multiwalled CNTs (having diameter 10-30 nm) were acquired from Sun Nanotech Co. Ltd. China, while the orange dye was bought from Sigma Aldrich (CAS Number 31482-56-1). The orange dye ($C_{17}H_{17}N_5O_2$) is an organic semiconductor material having density 0.9 g/cm^3 and molecular weight 323.35 g/mol. The OD's IUPAC name is 3-[N-Ethyl-4-(4-nitrophenylazo)phenylamino]propionitrile and it has p-type conduction. To make the substrates were made from rubber that is available commercially. The mortar and pestle were used to mix OD and CNTs (1:1 by weight) powders. The rubber substrates have the dimensions 12x5x5 mm^3. The CNTs-OD mixture was rubbed-in in the 3 mm width in the middle of the rubber substrate to form the rubber-CNTs-OD nanocomposite layer. The thickness of the rubber- CNTs-OD nanocomposite films in the different samples were in the range of 12-18 µm. The schematic illustration of the rubbing in process is shown in Fig.1. By using same process, the CNTs powder was rubbed-in on both sides of rubber-CNTs-OD nanocomposite layer to form rubber-CNTs nanocomposite, which worked as contact electrodes. The front and top views of the fabricated sensors are shown in Fig.2a and 2b, respectively. The detail about the rubbing-in technology is given our previous [33-35]. The same technique was used to fabricate the sensor under the pressure of 40 g/cm^2.

For the characterization of rubber-CNTs-OD nanocomposite layer the Philips PW1830 X-ray diffractometer (XRD) was used. The characterization was done using Cu-Kα radiation in θ-2θ (Bragg-Brentano) scanning mode at room temperature. The confirm the reproducibility of the results the samples were scanned three times.

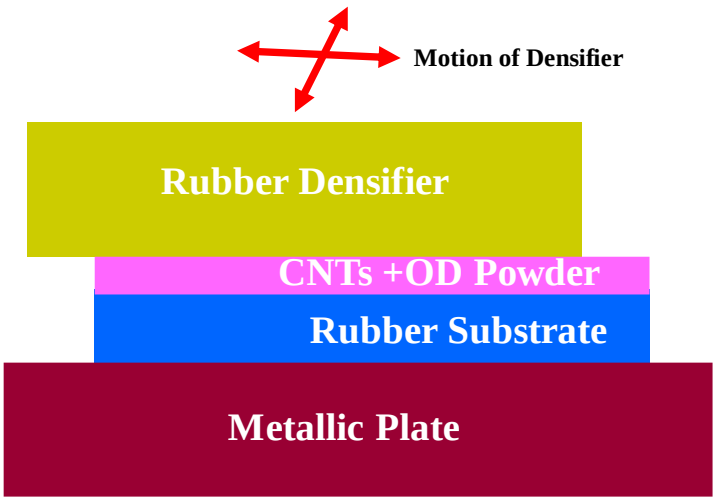

Figure 1. Schematic diagram of the rubbing-in technology used to fabricate rubber-CNTs-OD nanocomposite based multifunctional sensors.

For the displacement, pressure and force measurements the simple laboratory equipment's were used. Particularly, for the displacement the micrometer setup was used, while the pressure and force were created by applying the mechanical loads. In the case of experiments where the force was applied, the two cylindrical elements fabricated by dielectric material having diameter of 6 mm (No.1) and 2 mm (No.2) and length of 2 cm were used. During experiments the cylindrical element was placed perpendicular to long axis of the sample along of rubber-CNTs-OD nanocomposite layer. The schematic illustration of the applied pressure, displacement and force to the multifunctional resistive/impedimetric sensor is shown in Fig. 2C. The fabricated sensors were also tested for the humidity and temperature sensing. For this purpose indigenously made humidity and temperature testing set-ups were used.

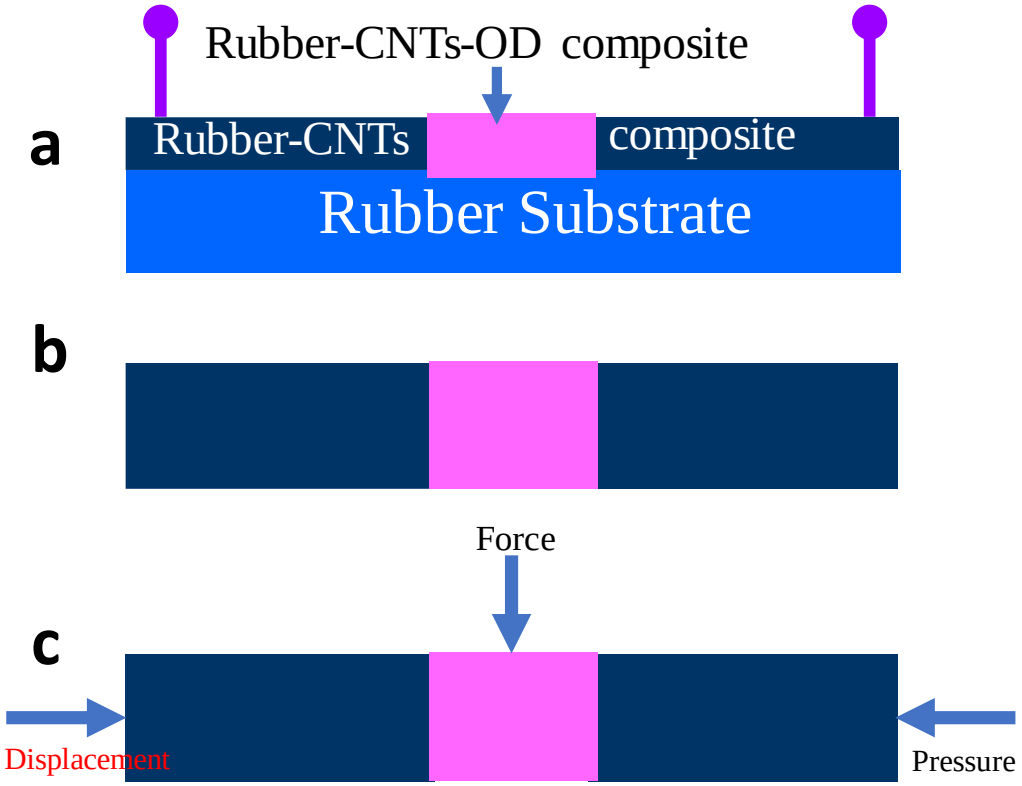

Figure 2. The schematic diagrams of the multifunctional resistive sensor: side view (a) and top view (b) and the illustration of the applied pressure, displacement and force on the sensor (c).

For the measurements of resistance and impedance the Fluke 87 multimeter and the digital LCR meter MT-4090 were used, respectively. The temperature and humidity were measure by TECPEL 322. The samples were placed in the chamber for investigation of the temperature and humidity effects. The displacement and pressure were created and measured by laboratory pressurizing and micrometric mechanisms.

3. RESULTS AND DISCUSSION

Figure 3 shows the XRD spectra of rubber, OD and CNTs. In the rubber spectrum the strong peaks at 2θ angle of 36°, 29.4° and 23.1° along with other peaks corresponds highly ordered polyvinyl chloride chains [16]. A major peak in CNTs spectrum at 26.2° (002) In XRD spectrum of CNTs, the major peak at 26.2° (002) corresponds to hexagonal graphite, which is comparable to ICSD code: 031170 (standard XRD data). The peak at 38.4° indicates the attachment of any functional group. The peak consistent with other studies [36] was also observed at 2θ of 44.3° (101). In OD spectrum the observed peaks are consistent with data presented in the refs. [37-39].

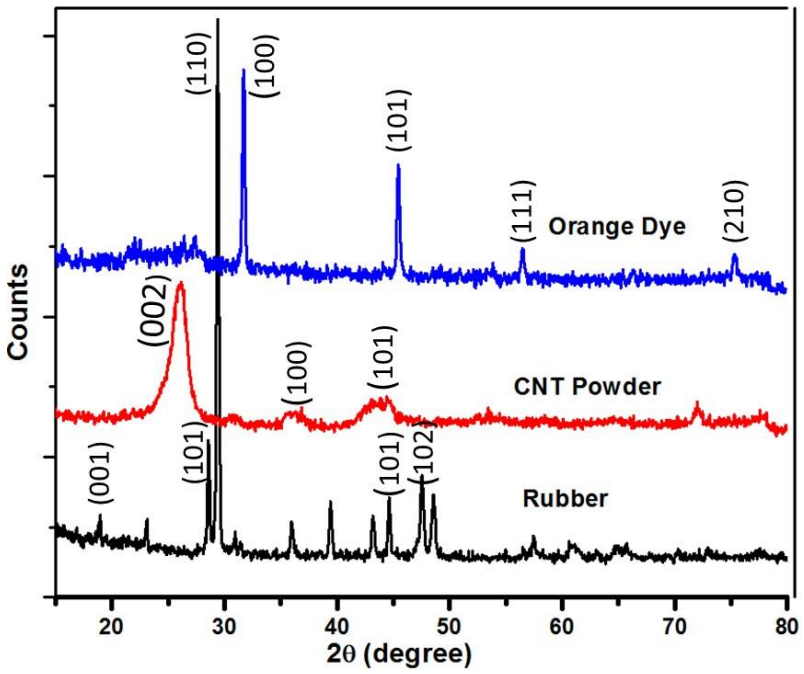

Figure 3. X-Ray diffraction patterns of rubber, CNT and orange dye.

Fig.4 shows resistance-displacement and impedance-displacement relationships of the rubber-CNTs-OD nanocomposite based multifunctional sensors. It is seen that as the compressive displacement increases the resistance and impedance of the sensor decrease. The sensor shows linear behavior. It is also evident from Fig.4b that on increasing frequency the initial impedance of the sensor decreases. The sensor's compressive displacement sensitivity (S_D) is calculated using the following equation:

$$S_D = (\Delta R \text{ or } \Delta Z)/D \quad (1)$$

Where, ΔR, ΔZ, D are the change in resistance, impedance and the displacement. The calculated values of sensitivity (S_D) are equal to -73 Ω/μm, -70 Ω/μm, -67 Ω/ μm, -63 Ω/μm, -53 Ω/ μm and -43 Ω/ μm on average at frequencies of 0 Hz,100Hz, 1kHz, 10kHz, 100kHz and 200kHz, respectively.

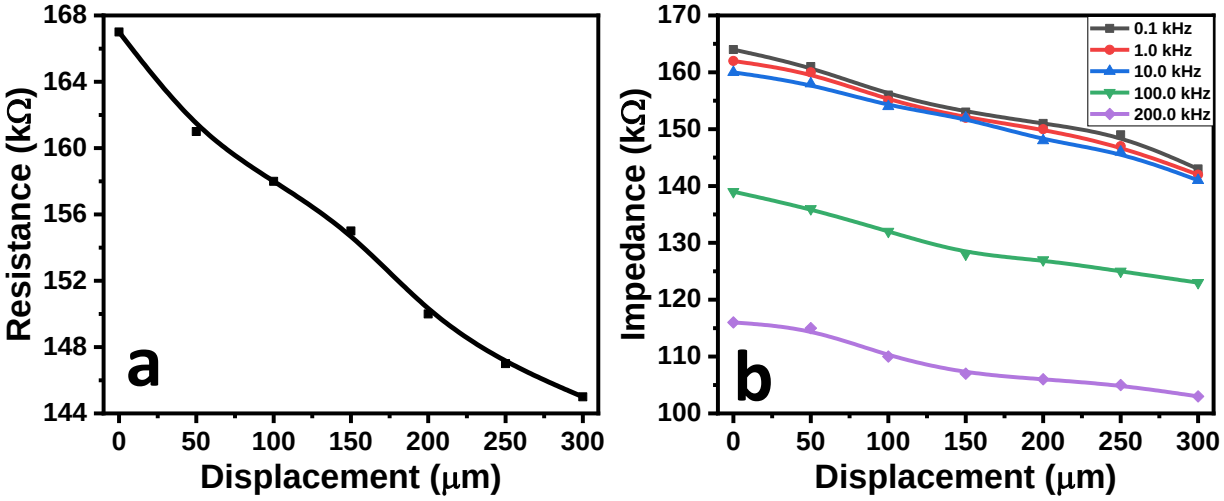

Figure 4. Resistance-displacement (a) and impedance-displacement (b) relationships of the rubber-CNTs-OD nanocomposite based multifunctional sensors.

Firstly, the sensitivity of the device to compressive displacement is negative because as displacement increases the resistance and impedances decrease. Secondly, it is seen that the compressive displacement sensitivity is decreasing with increase of the frequency. It may be explained by the contribution of capacitive component in the impedance: with increasing frequency the capacitive component of the impedance can partly "short circuit" the resistance of the sensor. The following simplified equivalent circuit (Fig.5) can represent the electric circuit of the sensor.

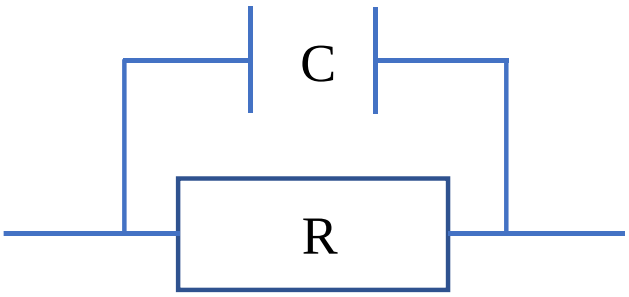

Figure 5. Equivalent circuit of the multifunctional sensor.

The relative resistance-pressure and the relative impedance-pressure relationships of the rubber-CNTs-OD nanocomposite relationships are shown in Fig.6. It can be seen that with increase in uniaxial pressure the resistance and the impedance of the sensor also decrease. It is similar behavior like in compressive displacement sensing. The pressure sensitivity (S_p) of the sensor can be determined by the following equation:

$$S_P = (\Delta R \; or \; \Delta Z)/p \qquad (2)$$

Where, p is the applied uniaxial pressure. The sensitivities (S_p) are found in the range of -6080 Ω-cm^2/kgf to -3950 Ω-cm^2/kgf on average in the frequency range of 100 Hz to 200 kHz. From this data it is revealed that the pressure sensitivity is frequency dependent: it decreases considerably at higher frequency (200kHz).

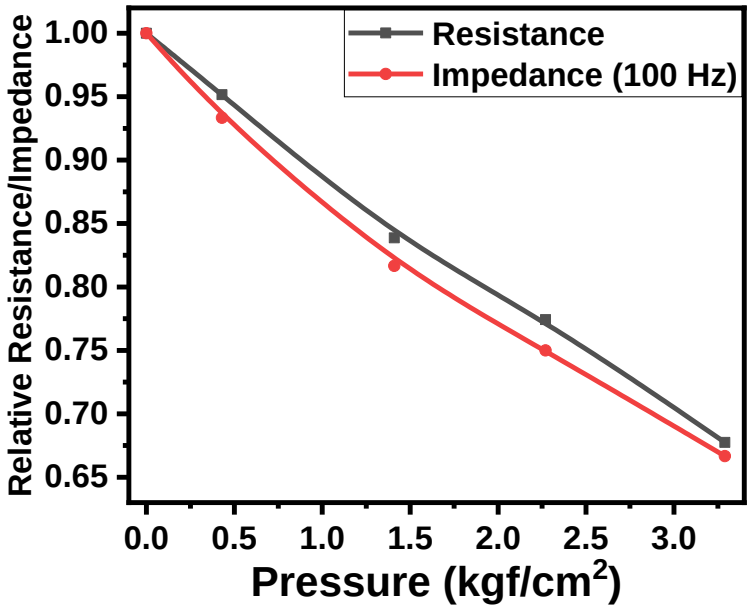

Figure 6. Relative Resistance-pressure and relative impedance-pressure relationships of rubber-CNTs-OD nanocomposite-based sensors.

In the cases of the compressive displacement and pressure the decrease in the resistance and the impedances may be due to the decrease in the distances between particles of OD and CNT. The squeezing of the particles may cause to change the geometrical parameters, decrease the intrinsic resistance and increase micro-capacitance between the particles as well.

The Fig.7 and Fig.8 present the effect of force on the resistance and the impedance of the rubber-CNTs-OD nanocomposite-based sensors using cylindrical pressing elements No.1 and No.2, respectively. The sensors were tested for force sensing in the range of 0 to 329 gf at various frequencies up to 200 kHz. It may be seen in Fig.7 and Fig.8 that the on increasing force the both the resistance and the impedance of the sensors increase.

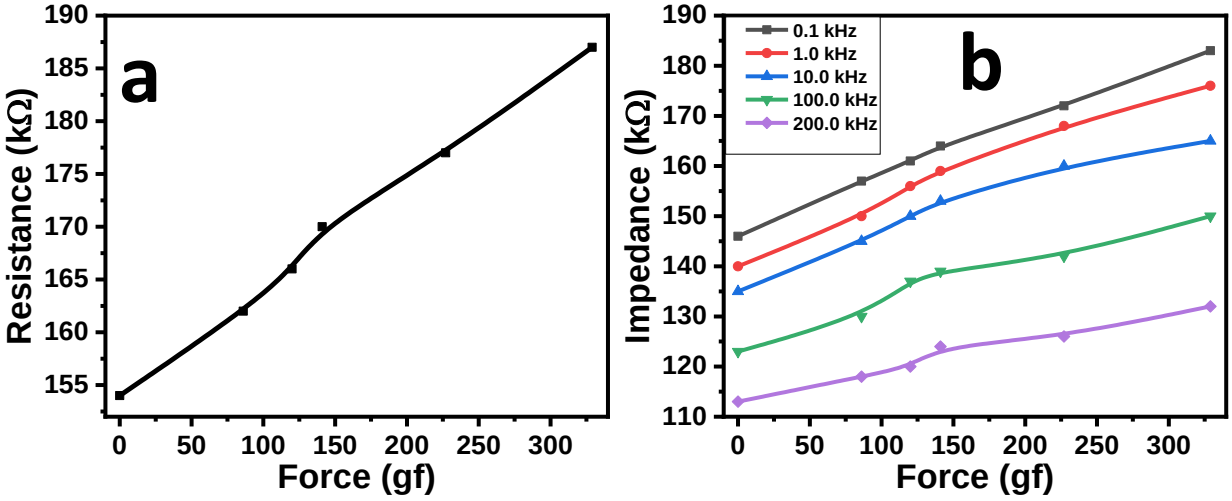

Figure 7. The resistance-force (a) and the impedance-force (b) relationships of rubber-CNTs-OD nanocomposite-based multifunctional sensors when tested using element No.1.

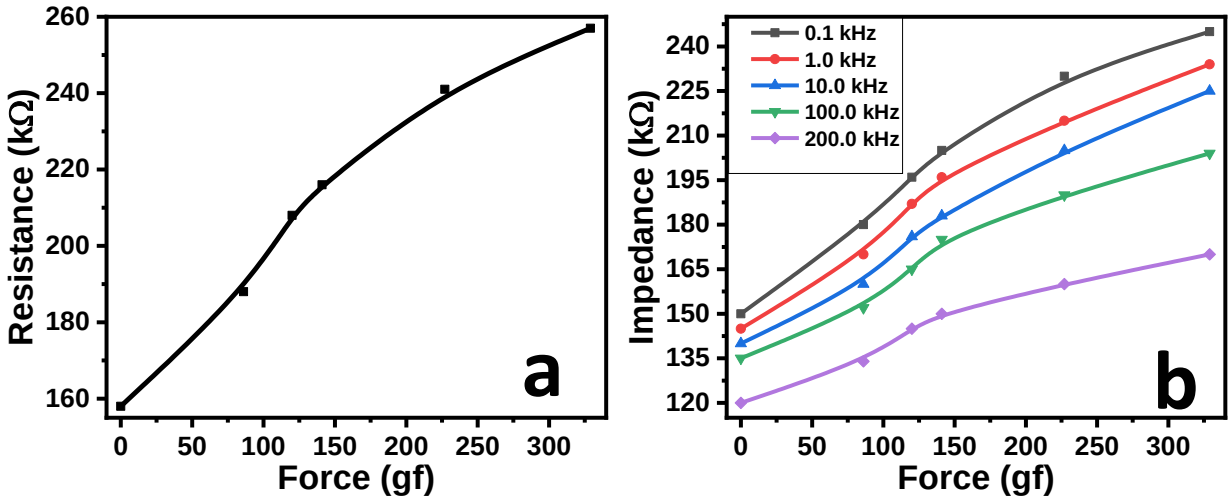

Figure 8. The resistance-force (a) and the impedance-force (b) relationships of rubber-CNTs-OD nanocomposite-based multifunctional sensors when tested using element No.2.

The force sensitivity (S_f) of the rubber-CNTs-OD nanocomposite-based sensors can be determined by the following equation:

$$S_f = (\Delta R \text{ or } \Delta Z)/f \quad (3)$$

where f is force in *gf*. When tested with element No.1 in the frequency range of 0 to 200 kHz, the calculated force sensitivities of the rubber-CNTs-OD nanocomposite-based sensors are in the range of 100 Ω/gf to 60 Ω/gf on average. The force sensitivities of the rubber-CNTs-OD nanocomposite-based sensors are found in the range of 300 Ω/gf to 150 Ω/gf when tested with element No.2 in frequency range of 0 to 200 KHz. The relative standard deviation in force, displacement and pressure sensing was calculated on the base of 4 readings and was found ±1.5% to ±2.5% depending on the measuring frequency. The loading-unloading behavior of the sensors was studied. It was found

that the sensors showed negligible hysteresis on application and withdrawn of force, displacement or pressure.

Comparison of the force applied through cylindrical element No.1 (Fig.7) and through cylindrical element No.2 (Fig.8) shows that the sensor demonstrates 3 times more sensitivity in case of element No.2 than in case of element No.1. This higher sensitivity is probably due to the higher pressure at the same force because of lower area of the pressing element in the case of element No.2. It should be emphasized that in these experiments unlike to previous one (pressure and compressive displacement), in this case the sensing element was under deformation of tension.

The humidity and temperature sensing behavior of the rubber-CNTs-OD nanocomposite-based sensors is shown in Fig. 9. On increasing humidity, the resistance and impedance of the sensors decease. The sensors show sensitivity in the humidity range of 40% to 93 % RH. It is evident from Fig. 9a that the change in impedance (Z) is higher than the change in resistance (R) in response to humidity. This indicates that humidity also causes significant change (increase) in the capacitance (C) of the sensor, which in turn causes higher reduction in the impedance. So, the value of impedance depends upon both the capacitance and the resistance, which are correlated by this equation ($Z=R/(1 + j\omega RC)$, where ω is angular frequency) [40]. The resistance-humidity and impedance-humidity sensitivities (S_H) were measured using the following expression:

$$S_H = (\Delta R \text{ or } \Delta Z)/\Delta H \quad (4)$$

Where, ΔR, ΔZ and ΔH are the change in resistance, impedance and humidity, respectively.

The rubber-CNTs-OD nanocomposite-based sensors show resistance-humidity sensitivity -187 Ω/%RH and impedance-humidity sensitivity up to -981 Ω/%RH. The relative standard deviation in humidity sensing was calculated on the base of 5 readings and was found ±2.1% on average. Moreover, absorption desorption was also studied and sensors showed a very small hysteresis (1.5 %).

This change in resistance and impedance may be regarded to the adsorption and absorption of water molecules at the surface of rubber-CNTs-OD nanocomposite. Further explanation regarding the humidity sensing mechanism is given in ref. [21].

The temperature sensing behavior of the rubber-CNTs-OD nanocomposite-based sensors is shown in Fig. 9b. The sensors were tested in the temperature range of 28 to 65 °C. It can be seen that both the impedance and resistance of the sensor decreases with increase in temperature, which is semiconducting behavior. The change in impedance is higher as compared to change in resistance in response to temperature change. The temperature sensitivity (S_T) of the sensors can be calculated by the following relationship:

$$S_T = (\Delta R \text{ or } \Delta Z)/\Delta T \quad (5)$$

Where, ΔT is the change in temperature. The average sensitivity was calculated and found in the range of -216 Ω/°C to -270 Ω/°C. Using data obtained by 4 readings the relative standard deviation was found ±2.45%. During temperature sensing a small hysteresis was observed which was calculated about 3.5%. This hysteresis may be regarded to insulating nature of the rubber which takes time to dissipate heat to ambient environment. The comparison of properties of fabricated sensors with the already reported sensors is given in Table-1.

The fabricated rubber-CNTs-OD nanocomposite-based multifunctional sensors have the ability to measure displacement, pressure, force, humidity and temperature. Out of these the pressure sensing

plays very important role, not only for industrial application but for environmental monitoring and evaluation [7-10, 41, 42].

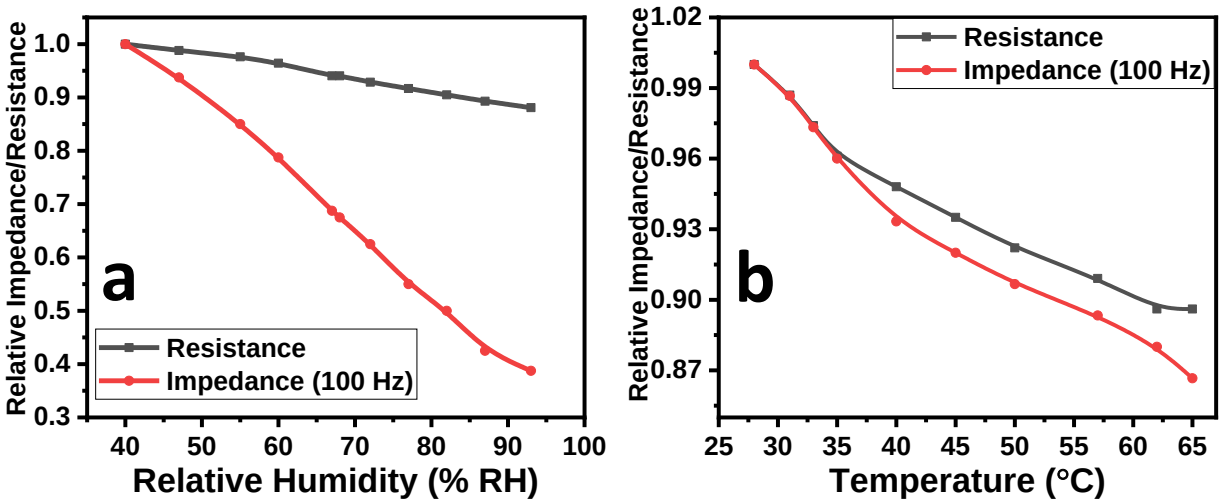

Figure 9. Humidity and temperature sensing behavior of the rubber-CNTs-OD nanocomposite-based sensors.

Table 1. Comparison of the properties of fabricated sensors with the already reported sensors

Sr. No		Fabrication Technology	Sensing Materials	Sensing Range	Sensitivity	Ref.
Temperature	1	Glued film	CNTs	20-75 °C	-0.272 Ω/°C	[43]
	2	Coating and sputtering	Silk fibron-AgNWs	20-60 °C	-0.125 Ω/°C	[44]
	3	Rubbing-in	Rubber-CNTs-OD	28-65 °C	-270 Ω/°C	Current Study
Displacement	1	Powder testing sensor	CNT-Graphene	0-100 µm	-0.17 Ω/µm	[14]
	2	Powder testing sensor	CNT-OD-Graphene	0-110 µm	-14.0 Ω/µm	[45]
	3	Rubbing-in	Rubber-CNTs-OD	0-110 µm	-73 Ω/µm	Current Study
Pressure	1	Powder testing sensor	CNT	0-1.86 gf/cm^2	645.2 Ω cm^2/gf	[46]
	3	Pressing	CNT-Cu_2O	0-378 gf/cm^2	0.009 Ω cm^2/gf	[47]
	3	Rubbing-in	Rubber-CNTs-OD	0-3290 gf/cm^2	-6.08 Ω cm^2/gf	Current Study

4. CONCLUSION

The multifunctional sensors were fabricated by simple and economical method, namely, rubbing-in technology. Materials which were used in the sensors (carbon nanotube, rubber and organic semiconductor orange dye) are available in the market. The sensors are shockproof and multifunctional. The displacement, pressure, force, humidity and temperature sensitivities are up to -73 Ω/μm, -6080 Ω-cm^2/kgf, 300 Ω/gf, -981 Ω/%RH and -270 Ω/°C, respectively. The sensitivities of the sensors are enough for practical application. The experiments showed that the sensors are reliable and can be used in practice and as teaching aid as well. It should be mentioned that the sensitive elements (OD and CNT) films were also fabricated by simple and economical method rubbing-in technology.

ACKNOWLEDGEMENTS
This project was funded by the Deanship of Scientific Research (DSR), King Abdulaziz University, Jeddah, Saudi Arabia under grant no. (KEP-13-130-41). The authors, therefore, acknowledge with thanks DSR technical and financial support.

COMPLIANCE WITH ETHICAL STANDARDS

CONFLICT OF INTEREST
The authors declare that they have no conflict of interest.

FUNDING
(Not applicable)

AVAILABILITY OF DATA AND MATERIAL
(Not applicable)

CODE AVAILABILITY
(Not applicable)

References

1. A. Garcia-Valenzuela and M. Tabib-Azar, in *Integrated Optics, Microstructures, and Sensors*, Springer US, Boston, MA, (1995) 267.
2. C.-L. Cheng, H.-C. Chang, C.-I. Chang and W. Fang, *J. Micromech. Microeng.*, 25 (2015) 125024.
3. D. Jones, L. Wang, A. Ghanbari, V. Vardakastani, A.E. Kedgley, M.D. Gardiner, T.L. Vincent, P.R. Culmer and A. Alazmani, *Sens.*, 20 (2020) 1123.
4. H. Lee, J. Chung, S. Chang and E. Yoon, *J. Microelectromech. Syst.*, 17 (2008) 934.
5. K. Flores De Jesus, M.H. Cheng, L. Jiang and E.G. Bakhoum, *J. Sens.*, 2015 (2015) 647427.
6. M. Laurenti, D. Perrone, A. Verna, C.F. Pirri and A. Chiolerio, *Micromach.*, 6 (2015) 1729.
7. V. Kraz, US Patents, US 6,614,235 B2. (2003).
8. R.A. Fernandes, US Patents, US 4801937A (1989).
9. M. Haefke, S.C. Mukhopadhyay and H. Ewald, in *2011 IEEE International Instrumentation and Measurement Technology Conference*, (2011) 1.
10. M.A.M. Yunus and S.C. Mukhopadhyay, *Meas. Sci. Technol.*, 22 (2011) 025107.

11. V. Kumar, G. Lee, K. Singh, J. Choi and D.-J. Lee, *Sens. Actuators A*, 303 (2020) 111712.
12. V. Kumar, R.-R. Wu and D.-J. Lee, *Polym. Compos.*, 40 (2019) E373.
13. V. Kumar, G. Lee, Monika, J. Choi and D.-J. Lee, *Polym.*, 190 (2020) 122221.
14. M.T.S. Chani, K.S. Karimov and A.M. Asiri, *Semicond.*, 54 (2020) 85.
15. K.S. Karimov, M. Riaz and J.-U. Nabi, *J. Therm. Anal. Calorim.*, 143 (2021) 3033.
16. I.P. Ejidike, C.W. Dikio, D. Wankasi, E.D. Dikio and F.M. Mtunzi, *Int. J. Environ. Stud.*, 75 (2018) 932.
17. A.M. Asiri and M.T.S. Chani, US 10317356, USA, (2019).
18. M. Chani, K.S. Karimov, K.S. KARIMOV, J.-U. NABI, A. AHMED, I. KIRAN and A. ASIRI, *J. Optoelectron. Adv. Mater.*, 21 (2019) 588.
19. M.T.S. Chani, *Microchim. Acta*, 184 (2017) 2349.
20. M.T.S. Chani, K.S. Karimov and A.M. Asiri, *Semicond.*, 53 (2019) 1622.
21. M.T.S. Chani, K.S. Karimov and A.M. Asiri, *J. Mater. Sci.: Mater. Electron.*, 30 (2019) 6419.
22. M.T.S. Chani, K.S. Karimov, A.M. Asiri, N. Ahmed, M.M. Bashir, S.B. Khan, M.A. Rub and N. Azum, *PLoS One*, 9 (2014) e95287.
23. M.T.S. Chani, K.S. Karimov, E.M. Bukhsh and A.M. Asiri, *Int. J. Electrochem. Sci*, 15 (2020) 5076.
24. M.T.S. Chani, K.S. Karimov, F. Khalid, S. Abbas and M. Bhatty, *Chin. Phys. B*, 22 (2013) 010701.
25. M.T.S. Chani, K.S. Karimov, F.A. Khalid, K. Raza, M.U. Farooq and Q. Zafar, *Physica E,* 45 (2012) 77.
26. M.T.S. Chani, K.S. Karimov, S.B. Khan, N. Fatima and A.M. Asiri, *Ceram. Int.*, 45 (2019) 10565.
27. M.T.S. Chani, S.B. Khan, A.M. Asiri, K.S. Karimov and M.A. Rub, *J. Taiwan Inst. Chem. Eng.*, 52 (2015) 93.
28. M.T.S. Chani, S.B. Khan, K.S. Karimov, M. Abid, A.M. Asiri and K. Akhtar, *J. Semicond.*, 36 (2015) 023002.
29. A.M. Asiri, M.T.S. Chani and S.B. Khan, US Patents, US 9,976,975, (2018).
30. M.T. Saeed, K.S. Karimov, F.A. Khalid, M. Farooq and M. Saleem, in *2011 Saudi International Electronics, Communications and Photonics Conference (SIECPC)*, IEEE, (2011) 1.
31. M.T.S. Chani, K.S. Karimov, H.M. Marwani, M.M. Rahman and A.M. Asiri, *Appl. Phys. A*, 127 (2021) 236.
32. M.T.S. Chani, K.S. Karimov, H.M. Marwani, M.M. Rahman and A.M. Asiri, *Int. J. Electrochem. Sci.* 16 (2021) 210566.
33. K.S. Karimov, N. Fatima, K.J. Siddiqui and M.I. Khan, *Mater. Sci. Energy Technol.*, 2 (2019) 551.
34. K.S. Karimov, Z. Ahmad, M.I. Khan, K.J. Siddiqui, T.A. Qasuria, S.Z. Abbas, M. Usman and A.-U. Rehman, *Heliyon*, 5 (2019) e01187.
35. M.T.S. Chani, K.S. Karimov, E.M. Bukhsh and A.M. Asiri, *Int. J. Electrochem. Sci*, 15 (2020) 5076.
36. Y. Lu, X. Liu, W. Wang, J. Cheng, H. Yan, C. Tang, J.-K. Kim and Y. Luo, *Sci. Rep.*, 5 (2015) 16584.
37. J.J. Ritter and P. Maruthamuthu, *Inorganic Chemistry*, 36 (1997) 260.
38. K.S. Karimov, M. Saleem, Y. Iqbal, N. Fatima and R. Gohar, *Appl. Phys. A*, 123 (2017) 740.
39. C. Muhammad Tariq Saeed, K.S. Karimov, H. Meng, K.M. Akhmedov, I. Murtaza, U. Asghar, S.Z. Abbass, R. Ali, A.M. Asiri and N. Nawaz, *Russ. J. Electrochem.*, 55 (2019) 1391.
40. J.D. Irwin and C.-H. Wu, *Upper Saddle River, NJ: Prentice-Hall, Inc, 1999.*, (1999).
41. I.U.r.I. Posudin, *Methods of measuring environmental parameters*, Wiley Online Library, (2014).
42. A.J. Both, L. Benjamin, J. Franklin, G. Holroyd, L.D. Incoll, M.G. Lefsrud and G. Pitkin, *Plant*

Methods, 11 (2015) 43.
43. K.S. Karimov, M.T.S. Chani and F.A. Khalid, *Physica E*, 43 (2011) 1701.
44. X. Qin, Y. Peng, P. Li, K. Cheng, Z. Wei, P. Liu, N. Cao, J. Huang, J. Rao, J. Chen, T. Wang, X. Li and M. Liu, *Int. J. Optomechatron.*, 13 (2019) 41.
45. S. Shafique, K.S. Karimov, M. Abid, M.M. Ahmed, K.M. Akhmedov and R. Aziz ur, *J. Mater. Sci.: Mater. Electron.*, 31 (2020) 8893.
46. A. Ali, A. Khan, K.S. Karimov, A. Ali and A. Daud Khan, *J. Nanomater.*, 2018 (2018) 9592610.
47. K.S. Karimov, M.T.S. Chani, F.A. Khalid, A. Khan and R. Khan, *Chin. Phys. B*, 21 (2012) 016102.